Volume 1 | Number 1 | Jan 2013 | Pages 1–100

Journal of
Materials Chemistry A

Materials for energy and sustainability
www.rsc.org/materialsA

Li⁺

ROYAL SOCIETY
OF CHEMISTRY

ROYAL SOCIETY
OF CHEMISTRY

www.rsc.org/materialsA

Time-Resolved Microwave Conductivity Study of Charge Carrier Dynamics in Commercially Available TiO$_2$ Photocatalysts

Shohei Nakajima and Ryuzi Katoh*

Department of Chemical Biology and Applied Chemistry, College of Engineering,

Nihon University, Koriyama, Fukushima 963-8642, Japan

(rkatoh@chem.ce.nihon-u.ac.jp)

Abstract

Charge carrier dynamics in various commercially available TiO$_2$ photocatalysts was studied by means of the time-resolved microwave conductivity (TRMC) technique. The intensities of the TRMC signals strongly depended on the photocatalyst, suggesting that the TRMC technique is potentially useful for characterizing photocatalytic activity. We found that fast charge recombination within the time resolution of the measurement system becomes dominant when one or more charges are generated primarily in a particle. We also found that the TRMC signals were sensitive to the particle size and that the maximum signal intensity was roughly proportional to the diameter of the particles. This tendency was explained on the basis of a model in which electron traps are located at the surface of the particles. P25, one of the best photocatalysts developed to date, showed a slight deviation from this tendency; the reason for the deviation is discussed.

Introduction

Photocatalysts based on TiO$_2$ have attracted much attention as promising environmental photocatalysts, and a huge number of studies have been carried out on these materials.[1-3] Currently, various commercially available products with widely varying photocatalytic activities are utilized in various applications. The surface properties of the TiO$_2$ particles, which sensitively depend on the conditions under which they are prepared, are the limiting factor for their photocatalytic activity. Various attempts to clarify the relationship between the photocatalytic activity and the physical properties of TiO$_2$ photocatalysts such as surface area, particle diameter and crystal structure have been carried out.[4,5] However, so far, no clear relationship has been obtained. Thus, the primary processes of the photocatalytic reaction must be evaluated for a detailed study.

The transient absorption (TA) technique has been widely employed to study primary processes in photocatalysts.[6-16] Reactive species can be assigned from TA spectra, and trapped holes, trapped electrons and quasi-free electrons have been identified.[9] The rate of recombination of electrons and holes can be evaluated from decay profiles. The recombination rate increases with increasing density of charges produced in a particle, and slow recombination within the microsecond time region can be observed under weak-excitation conditions.[9,15] If the reaction is an efficient process, the reaction rate and

yield can also be evaluated by TA measurements. Holes produced in a particle react with methanol with almost unity efficiency, and the reaction is very fast (rate constant 1/300 ps).[11] In contrast, reaction of electrons with oxygen is slow (on the order of milliseconds).[14,15]

In principle, it is possible to apply the TA technique to clarify the factors responsible for the differences in the photocatalytic activities among commercial products. However, commercial products are powders, and scattering of the probe light is a serious problem in evaluating primary processes quantitatively. To address this problem, TA measurements have been made using long-wavelength light. Onishi and co-workers studied infrared detection of transient species produced in TiO_2 particles under UV excitation.[12] They evaluated photocatalytic reaction rates for several commercial products and found differences in TA signal intensities and recombination rates.[12] Although the factors responsible for these differences are not fully understood, it is quite important to identify them.

Long-wavelength detection of TA signals can also be accomplished by using microwave or terahertz electromagnetic waves. The origin of the TA signal in the microwave to terahertz region is different from that in the visible to infrared region. In the visible to infrared region, absorption is induced by the optical transition from the ground state to the excited state of the transient species produced by light excitation. In contrast, in the microwave to terahertz region, absorption is proportional to the conductivity of the charge carriers produced in the sample, *i.e.*, the number of mobile charges multiplied by the mobility of the charge. Although the microwave and terahertz TA techniques are useful for studying the primary processes in TiO_2 photocatalysts, the terahertz TA technique is not commonly used because of experimental difficulties.[17] In contrast, in the microwave TA technique, time-resolved microwave conductivity (TRMC) is relatively easy to measure, and thus the TRMC technique is suitable for systematic study of various TiO_2 samples.

The first TRMC study of TiO_2 was carried out in 1984;[18] since then, several groups have used the TRMC technique to study charge carrier dynamics in TiO_2 nanoparticles.[19–26] The TRMC signal is very sensitive to the particle size and morphology of the sample; for example, the TRMC signal of small particles (d < 20 nm) is three orders of magnitude smaller than that of thin films.[19,20] A recent study suggests that this remarkable difference is due to a difference in the efficiency of detecting charge carriers; *i.e.*, the trapping process plays an important role in TRMC measurements of TiO_2.[24] Although several crystal structures are known for TiO_2, the anatase and rutile structures are common for commercially available TiO_2 powders. Because the TRMC signals from these structures are very different,[25] the TRMC technique has been used to elucidate charge carrier dynamics and reaction processes in TiO_2 photocatalysts.[22]

Although the TRMC technique is potentially a powerful tool for studying charge carrier dynamics in TiO_2, the relationship between the TRMC signal and various basic properties of TiO_2 is not fully

understood. To overcome this problem, a systematic TRMC study of TiO_2 photocatalysts is needed. Commercial products are good candidates for study because the properties of laboratory-prepared TiO_2 photocatalysts are often sensitive to the preparation method. Thus, we carried out a systematic TRMC study of several commercially available TiO_2 photocatalysts for which basic properties such as particle size are available. Accordingly, we can discuss the relationship between the TRMC signal characteristics and the basic properties of TiO_2 photocatalysts.

Experimental

Commercial TiO_2 photocatalysts were used as sample materials (Table 1). All samples were used as obtained from the suppliers. The diameters of the TiO_2 photocatalyst particles (*d*) and ratios of the rutile to anatase structures (*R/A*) are listed in Table 1. A powder scraped from a nanoporous nanocrystalline TiO_2 films was used as a standard sample for evaluating the absolute value of the conductivity. This film has been used as an electrode for dye-sensitized solar cells[27] and the films were prepared by screen-printing a TiO_2 paste containing nanoparticles (*d* = 9 nm; Ti-Nanoxide HT/SP, Solaronix) onto glass slides and then calcining the printed substrates for 1 h at 800 K.

TRMC measurements were carried out with homemade TRMC equipment.[28] Microwaves were generated by an oscillator based on a 200-mW Nakadai MGS-15B Gunn diode. The oscillator was equipped with a varactor diode, which was used to tune the frequency of the microwaves from 8.5 to 10 GHz (X-band). The microwaves traveled toward the sample cavity through a circulator. The sample cavity was placed at the end of the waveguide as shown in Fig. 1. A powder sample in a 5-mm-diameter glass tube was placed in the cavity. Under the experimental conditions, the quality factor Q of the cavity was given by $Q = f_0 / \Delta f_0$, where f_0 is the resonant frequency of the cavity and Δf_0 is the full width at half maximum of the cavity resonance curve.[29] Actually, Q was estimated to be about 200, and the time resolution was about 20 ns. The third harmonic (355 nm) of a Lotis TII LS-2137 Nd^{3+}:YAG laser was employed for UV excitation. The duration of the laser pulse was about 10 ns. Reflected microwaves were detected with an NEC IN23WE diode. Signals were processed with a Tektronix TDS5032 digital oscilloscope and analyzed with a computer.

Results and discussion

Evaluation of the absolute value of the microwave conductivity

The TRMC technique is a type of TA spectroscopy that measures the conductivity σ of mobile charge carriers produced by pulsed light excitation.[19] The absorption of microwave power $-(\Delta P/P)$ can be expressed as

$$-\left(\frac{\Delta P}{P}\right) = K\sigma = K'\mu N_e, \tag{1}$$

where K and K' are a constant, μ is the mobility of the charge carriers, and N_e is the number of charges generated. The TRMC signal contains information about the mobility of charge carriers, which is different from conventional TA measurements in the visible to near-IR wavelength region. Thus, the time evolution of $-(\Delta P/P)$ gives information about the recombination or trapping of charge carriers. Just after excitation, N_e shows a maximum value and gives the charge generation efficiency Φ_{CG} of mobile charges. If excitation light is perfectly absorbed by the sample, eq. (1) can be rewritten as

$$-\left(\frac{\Delta P}{P}\right)_{max} \Bigg/ I_{ex} = K''\Phi_{CG}\mu, \qquad (2)$$

where K'' is a constant and I_{ex} is the intensity of the excitation light. K'' is sensitive to the excitation volume and thus the difference of excitation volume among samples should be considered for quantitative discussion. In the present study, TiO_2 powder samples were used. The penetration depth of the excitation light for TiO_2 at 355 nm is typically several micrometers as reported previously,[23] which is much smaller than the wavelength of the microwave (3.3 cm at 9 GHz). Although absorption coefficient is slightly different among different TiO_2 powders as reported previously,[30] the same K'' value can used for all samples. The Φ_{CG} values obtained in this way are often affected by the time resolution of the measurement system. If charge recombination occurs within the time resolution of the system, the Φ_{CG} value becomes smaller than the primary generation efficiency Φ_{pri}.

TRMC measurements were carried out on TiO_2 nanoparticles, and characteristic features were found. In eq. (2), mobility μ includes contributions from both electrons and holes. For TiO_2 nanoparticles, it has been argued that holes are trapped rapidly.[16] and therefore only the electron contribution is detected in TRMC measurements.[20] The $-(\Delta P/P)$ of electrons in a TiO_2 nanocrystalline film is not simply proportional to the excitation light intensity I_{ex}. The I_{ex} dependence is bell-shaped: i.e., $-(\Delta P/P)_{max}/I_{ex}$ values increase with increasing I_{ex} at low I_{ex}, reach a peak, and then decrease with increasing I_{ex}. According to previous studies,[19] the bell shape can be attributed to the trap-filling effect at low I_{ex} and to efficient fast recombination at high I_{ex}. The trap-filling effect can be explained as follows. At low I_{ex}, all generated electrons are effectively trapped, and their effective mobility becomes very small. The number of mobile electrons increases with increasing I_{ex} because the number of available unoccupied traps becomes progressively smaller as I_{ex} increases, and therefore a large TRMC signal is observed. At high I_{ex}, the TRMC signal decreases again because secondary recombination of electrons and holes occurs efficiently within the time resolution of the apparatus.

As shown in eq. (2), the absolute value of $\Phi_{CG}\mu$ should be evaluated for quantitative discussion. Although $\Phi_{CG}\mu$ can be evaluated numerically for TiO_2 thin films,[19] such evaluation is difficult for a powder sample in a tube that is contained within a cavity. As far as we know, no standard powder sample is

available for evaluating the absolute value of $\varPhi_{CG}\mu$. Therefore, as a standard sample (ST), we used the powder obtained by scraping a nanocrystalline TiO_2 thin film. We measured $-(\Delta P/P)_{max}/I_{ex}$ as a function of I_{ex} for ST and a powder sample of P25 under the same experimental conditions, *i.e.*, the same Q value of the cavity (Fig. 2). The absolute value of $\varPhi_{CG}\mu$ for nanocrystalline films has been evaluated as 0.015 cm^2 V^{-1} s^{-1} at the top of the bell-shaped dependence.[21] Thus, the absolute value of $\varPhi_{CG}\mu$ in P25 can be evaluated by comparison with the absolute value of $\varPhi_{CG}\mu$ in ST based on eq. (2) (Fig. 2).

For later discussion, two parameters, $[\varPhi_{CG}\mu]_{max}$ and $[I_{ex}]_{peak}$, are introduced. As shown in Fig. 2, $[\varPhi_{CG}\mu]_{max}$ and $[I_{ex}]_{peak}$ are defined as the $\varPhi_{CG}\mu$ value and the light intensity at the maximum of the bell-shaped dependence, respectively.

Decay profile of TRMC signal

It is often pointed out that the properties of photocatalysts are affected by thermal treatment.[22] The TRMC technique has been used to study the effect of thermal treatment of photocatalysts, and various mechanisms have been proposed to account for changes caused by thermal treatment, including increase in particle size and change in crystal structure from anatase to rutile.[22]. Irreversible change occurs dominantly at high temperature (>500 °C), whereas reversible changes have been observed in the decay profiles of TRMC signals of nanocrystallne TiO_2 films at low temperature (450 °C).[20] These results imply that the adsorption of water molecules on the photocatalyst surface plays an important role in TRMC measurements. In fact, water molecules physically adsorbed on TiO_2 surfaces are desorbed by thermal treatment at 150 °C.[31]

Figure 3 shows TRMC decay profiles for P25 (I_{ex} = 1.3 mJ cm^{-2}) and ST01 (I_{ex} = 1.5 mJ cm^{-2}) before and after thermal treatment at 300 °C for 1 h. The decay profiles for P25 were the same before and after thermal treatment within the margin of error (Fig. 3a). On the contrary, a significant thermal treatment effect can be seen for ST01 (Fig. 3b). Note that the change in TRMC signal for ST01 was irreversible. Similar to the case for P25, decay profiles for the other samples in Table 1 were essentially the same before and after thermal treatment, suggesting that water molecules physically adsorbed on the surface do not affect the motion of the electrons in these TiO_2 powder samples. In a previous study of ST01, remarkably different decay profiles were observed in the microsecond time region after thermal treatment at 600 °C for 3 h.[23] This result suggests that a marked crystallinity change, such as growth of a crystal domain in the particles, occurred in ST01 even at 300 °C. A detailed study to clarify the mechanism of this change is underway in our laboratory. Although the reason for the effect observed for ST01 is unclear, the following measurements were carried out without thermal treatment.

Figure 4 shows decay profiles of $-(\Delta P/P)$ for the TiO_2 samples listed in Table 1 (I_{ex} = 2 mJ cm^{-2}). The decay profiles were not sensitive to the excitation light intensity (data not shown), in agreement with results from a previous study on nanocrystalline TiO_2 films.[21] The decay profiles are similar to each other,

except for the profile for ST01, in which the signal decays quickly. Although there are no clear explanations for the fast decay of the ST01 profile, one possible explanation is that electrons are trapped by structural defects in the particles. As mentioned above, the TRMC decay profile for ST01 is strongly affected by thermal treatment, which is probably caused by growth of a crystal domain in the particles. This suggests that the crystallinity of ST01 particles is not perfect; in other words, amorphous-phase domains are included. Thus, trapping of electrons at the phase boundary is a possible reason for the fast decay.

It was found that the TRMC signal of rutile TiO_2 decays very rapidly compared with that of anatase TiO_2.[25] Thus, we examined TRMC measurements of the commercial products of rutile TiO_2. Figure 5 shows TRMC signals of G1, a rutile TiO_2 (Showa Titanium, d = 250 nm), and ST41, an anatase TiO_2 (Ishihara Sangyo, d = 200 nm). The TRMC signal of G1 decays rapidly, in agreement with previous results.[25] On the basis of TA results for the rutile single crystal in the visible wavelength range,[32] the recombination time is expected to be on the order of microseconds under this excitation condition. Thus, the fast decay of the TRMC signal of G1 reflects the trapping process, and the small long-lived signal of G1 would reflect population of electrons.

The P25, F1 and F2 powder samples contain the rutile phase (Table 1). Accordingly, a spike-like signal corresponding to the rutile phase is expected to be observed, as in Fig. 5. However, no such spike-like signal was observed for P25, F1 and F2 (Fig. 4). This result suggests that electron transfer from the rutile domain to the anatase domain occurs within the time resolution of the measurement system, as pointed out previously.[33]

Excitation intensity dependence of $\Phi_{CG}\mu$

Figure 6 shows $\Phi_{CG}\mu$ of TiO_2 samples listed in Table 1 as a function of I_{ex}. This clearly shows that the excitation dependence of $\Phi_{CG}\mu$ varies markedly among the TiO_2 samples. The I_{ex} dependence of all samples can be explained on the basis of a bell-shape dependence, similar to the case for P25 and ST (Fig. 2). The values of $[I_{ex}]_{peak}$ and $[\Phi_{CG}\mu]_{max}$ (Table 2) can be obtained from Fig. 6. Although some of the curves in Fig. 6 do not show a proper bell shape, but rather just a saturated tendency, the values of $[I_{ex}]_{peak}$ and $[\Phi_{CG}\mu]_{max}$ are estimated with relatively large error.

Previous studies of TRMC in TiO_2 particles have shown that the TRMC signal tends to increase with increasing particle size.[20] Values of $[I_{ex}]_{peak}$ and $[\Phi_{CG}\mu]_{max}$ are plotted as a function of the particle diameter d in Figs. 7 and 8, respectively. Figures 7 and 8 clearly show that the values of $[I_{ex}]_{peak}$ and $[\Phi_{CG}\mu]_{max}$ are correlated with d. It is obvious that $[I_{ex}]_{peak}$ is proportional to d^{-3} and that $[\Phi_{CG}\mu]_{max}$ is proportional to d. A model explaining these tendencies is discussed below.

As discussed above, $[I_{ex}]_{peak}$ is the onset intensity for fast charge recombination occurring within

the time resolution of the measurement system. Fast recombination would occur before trapping of both electrons and holes. Because the trapping time for holes is less than 100 fs in TiO_2 nanocrystalline films composed of nanoparticles of $d = 9$ nm,[16] the fast recombination observed here would occur rapidly, suggesting that the recombination is an intraparticle event. Because charge recombination is a second-order reaction, the number of electrons N_C generated in a particle is an important parameter (N_C is proportional to the volume of the particle V_p (= $(\pi d^3)/6$) for a given excitation light intensity). Hence, the observed d^{-3} dependence of $[I_{ex}]_{peak}$ means that fast charge recombination becomes dominant when the same number of electrons are generated in a particle. The number of charges $[N_C]_{peak}$ produced in a particle at $[I_{ex}]_{peak}$ can be evaluated using the density of the particle D_p (= $6P/\pi d^3$) and the excitation density $[D_{ex}]_{peak}$ at $[I_{ex}]_{peak}$:

$$\left[N_C\right]_{peak} = \frac{\left[D_{ex}\right]_{peak}}{D_P} = \frac{\Phi_{CG}\alpha\left[I_{ex}\right]_{peak}}{\left(6P/\pi d^3\right)} \,. \tag{3}$$

where P is the porosity of the powder sample and α is the absorption coefficient. Values of $\alpha = 1 \times 10^4$ cm^{-1} is used[23] and P is assumed to be 0.5. Accordingly, the dotted line in Fig. 7 represents the relation $N_C^{peak} = 1$, clearly indicating that fast intraparticle charge recombination efficiently occurs when one or more charge pairs are produced in a particle. Although this has been pointed out for small nanoparticles ($d = 9$ nm),[19] we note that such fast recombination also occurs under a similar electron density condition for large particles (*e.g.*, ST41 ($d = 200$ nm), F1 ($d = 90$ nm), F2 ($d = 60$ nm) and F4A ($d = 30$ nm)).

This fast recombination implies that the motion of electrons and holes in the particle is affected by charges trapped in the particle. As shown in Fig. 6, the trap-filling effect is dominant below $[I_{ex}]_{peak}$, suggesting that electrons and holes produced in the particle can be trapped efficiently. Under such conditions, slow recombination is expected. Above $[I_{ex}]_{peak}$, one or more charges are produced, and these charges undergo recombination before trapping; that is, the second-generated charge in the particle is difficult to trap. This suggests that the motion of the second-generated charge is affected by the electric field induced by trapped charges in the same particle.

$[\Phi_{CG}\mu]_{max}$ is the maximum value in the bell-shaped dependence of $\Phi_{CG}\mu$ on I_{ex}. According to the previous study on small TiO_2 nanoparticles ($d = 9$ nm), the gradual increase of $[\Phi_{CG}\mu]_{max}$ in the low-I_{ex} region can be explained by the trap-filling effect, which is suppressed by simultaneous UV light irradiation.[19] Under such conditions, the $\Phi_{CG}\mu$ value in the low-I_{ex} region becomes similar to $[\Phi_{CG}\mu]_{max}$, indicating that $[\Phi_{CG}\mu]_{max}$ is the $\Phi_{CG}\mu$ value free from the trap-filling effect. Thus, the $[\Phi_{CG}\mu]_{max}$ values obtained in the present study differ among the samples due to their different Φ_{CG} and μ values. Recently, the $\Phi_{CG}\mu$ value obtained from TRMC measurements of nanocrystalline films composed of anatase nanoparticles and anatase flat films was discussed by dividing into two contributions, i.e., Φ_{CG} and μ.

Accordingly, in both the nanocrystalline and flat films, the mobility was evaluated as μ = 1.7 cm^2 V^{-1} s^{-1}. The generation efficiency Φ_{CG} of TRMC-detectable charges was estimated to be Φ_{CG} = 0.02 in the nanocrystalline film, and Φ_{CG} = 1 in the flat film. For nanocrystalline films, the primary efficiency of charge generation is known to be Φ_{pri} = 1,[20] indicating that the majority of electrons are rapidly trapped and that the remaining electrons are detected by TRMC measurements. This suggests that the $\Phi_{CG}\mu$ values in Fig. 6 are mainly controlled by the generation efficiency Φ_{CG} of TRMC-detectable charges.

As discussed above, Φ_{CG} is related to the density of trap sites D_{trap}; thus, Φ_{CG} can be expressed as

$$\Phi_{CG} = \frac{D_{free}}{D_{photon}} = \frac{D_{pri} - D_{trap}}{D_{photon}} = \frac{\Phi_{pri} D_{photon} - D_{trap}}{D_{photon}} = 1 - \frac{D_{trap}}{D_{photon}}, \tag{4}$$

where D_{photon}, D_{free}, D_{pri} and D_{trap} are the densities of absorbed photons, detectable electrons, primary generated electrons and trapped electrons, respectively. Because the efficiency Φ_{pri} of primary generated electrons is almost unity, Φ_{CG} can be expressed as the right-hand-side of eq. (4). If we assume that trap sites are located only at the surface of the particle, D_{trap} is expressed as

$$D_{trap} = S_P D_{trap}^S D_P = \left(\frac{6P}{d} D_{trap}^s \right), \tag{5}$$

where S_P (= πd^2) is the surface area of the particle and D_{trap}^s is the density of traps per unit area of the surface of a TiO$_2$ particle. Thus, Φ_{CG} is expressed as

$$\Phi_{CG} = 1 - \frac{6P D_{trap}^s}{d D_{photon}}. \tag{6}$$

When Φ_{CG} is small compared with Φ_{pri}, Φ_{CG} is roughly proportional to d, which is consistent with the correlation shown in Fig. 8. This clearly indicates that the TRMC signal intensity from the TiO$_2$ powder sample is mainly controlled by the density of traps located on the surface of the particle. In other words, the traps for electrons are located only at the surface.

In Fig. 8, the data point for P25 slightly deviates from the straight line obtained by correlation of the data points of the other samples. This suggests that the trap density in P25 is lower than that in the other samples. P25 has a high photocatalytic activity and is one of the best photocatalysts developed to date.[5] The origin of the high photocatalytic activity of P25 is frequently attributed to the presence of the

rutile phase.[5] However, in the present study, F1 and F2, both of which contain a rutile phase, have about the same photocatalytic activity as that of samples containing only an anatase phase. Therefore, the presence of a rutile phase is a necessary but not sufficient condition to explain the high photocatalytic activity of P25.

Conclusion

We studied charge carrier dynamics in various commercially available TiO_2 photocatalysts by means of the TRMC technique. The intensities of the TRMC signals strongly depended on the photocatalyst, indicating that the TRMC technique is potentially useful for characterizing photocatalytic activity in TiO_2 photocatalysts. We found good correlation between $[I_{ex}]_{peak}$ and d, suggesting that charge recombination becomes dominant when one or more charges are generated primarily in a particle. $[\Phi_{CG}\mu]_{max}$ and d were well correlated, which was explained on the basis of a model in which traps are located only at the surface of TiO_2 particles. P25, which is one of the best photocatalysts developed to date, slightly deviated from the $[\Phi_{CG}\mu]_{max}$ *vs. d* straight line obtained by plotting data for other TiO_2 photocatalysts, suggesting that the TRMC technique can be used as a tool to explore novel photocatalysts with high activity.

Acknowledgements

References

1 M. R. Hoffmann, S. T. Martin, W. Choi and D. W. Bahnemann, *Chem. Rev.,* 1995, **95**, 69-96.

2 A. Fujishima, X. Zhang and D. A. Tryk, *Surf Sci. Rep*., 2008, **63**, 515.

3 B. Ohtani, *J. Photochem. Photob*iol. C, 2010, **11**, 157.

4 J. Ryu and W. Choi, *Environ. Sci. Technol.,* 2008, **42**, 294.

5 B. Ohtani, O. O. Prieto-Mahaney, F. Amao, N. Murakami and R. Abe, *J. Adv. Oxid. Technol.,* 2010, **13**, 247.

6 Bahnemann, D. W.; Hilgendorff, M.; Memming, R. *J. Phys. Chem. B,* 1997, **101**, 4265.

7 A. Furube, T. Asahi, H. Masuhara, H. Yamashita and M. Anpo, *Chem. Phy. Lett.,* 1997, **275**, 234.

8 J. Rabani, K. Yamashita, K. Ushida, J. Stark and A. Kira, *J Phys. Chem. B*, 1998, **102**, 1689.

9 T. Yoshihara, R. Katoh, A. Furube, Y. Tamaki, M. Murai, K. Hara, S. Murata, H. Arakawa and M. Tachiya, *J. Phys. Chem. B*, 2004, **108**, 3817.

10 I. A. Shkrob, M. C. Jr. Sauer and D. Gosztola, *J. Phys. Chem. B,* 2004, **108**, 12512.

11 Y. Tamaki, A. Furube, M. Murai, K. Hara, R. Katoh and M. Tachiya, *J. Am. Chem. Soc.*, 2006, **128**, 416.

12 A. Yamakata, T. Ishibashi and H. Onishi, *Chem. Phys.,* 2007, **339**, 133.

13 T. Tachikawa, M. Fujitsuka and T. Majima, *J. Phys. Chem. C*, 2007, **111**, 5259.

14 M. Murai, Y. Tamaki, A. Furube, K. Hara and R. Katoh, *Catal. Today*, 2007, **120**, 214.

15 J. Tang, J. R. Durrant and D. R. Klug, *J. Am. Chem. Soc.*, 2008, **130**, 13885.

16 Y. Tamaki, K. Hara, R. Katoh, M. Tachiya and A. Furube, *J. Phys. Che*m. C, 2009, **111**, 11741.

17 P. Tiwana, P. Parkinson, M. B. Johnston, H. J. Snaith and L. M. Herz, *J. Phys. Che*m. C, 2010, **114**, 1365.

18 J. M. Warman, M. P. de Haas, M. Grätzel and P. P. Infelta, *Nature*, 1984, **310**, 306.

19 J. E. Kroeze, T. Savenije, J. M. Warman, *J. Am. Chem. Soc.*, 2004, **126**, 7608.

20 R. Katoh, A. Huijser, K. Hara, T. J. Savenije and L. D.A. Siebbeles, *J. Phys. Chem. C*, 2007, **111**, 10741.

21 T. J. Savenije, A. Huijser, M. J. W. Vermeulen and R. Katoh, *Chem. Phys. Lett*., 2008, **461**, 93.

22 J. T. Carneiro, T. J. Savenije, J. Moulijn and G. Mul, J. *Phys. Chem.C,* 2011, **115**, 2211.

23 R. Katoh, A. Furube, K. Yamanaka and T. Morikawa, *J. Phys. Chem. Lett.*, 2010, **1**, 3261.

24 M. C. Fravventura, D. Deligiannis, J. M. Schins and L. D. A. Siebbeles, *J. Phys. Chem. C*, 2013, **117**, 8032.

25 C. Colbeau-Justin, M. Kunst and D. Huguenin, *J. Mater. Sci*., 2003, **38**, 2429.

26 A. Saeki, Y. Yasutani, H. Oga and Shu Seki, *J. Phys. Chem. C*, 2014, **118**, 22561.

27 A. Hagfeldt, G. Boschloo, L. Sun, L. Kloo and H. Pettersson, *Chem. Rev*., 2010, **110**, 6595.

28 R. Katoh, A. Furube, M. Kasuya, N. Fuke, N. Koide and L. Han, *Sol. Energy Mater. Sol. Cell*, 2009, **93**, 698.

29 M. P. De Haas and J. M. Warman, *Chem. Phys.* 1982, **73**, 35.

30 M. L. Satuf, R. J. Brandi, A. E. Cassano and O. M. Alfano, *Ind. Eng. Chem. Res.* 2005, **44**, 6643.

31 A. Nosaka and Y. Nosaka, *Bull. Chem. Soc. Jpn*., 2005, **78**, 1595.

32 R. Katoh, M. Murai and A. Furube, *Chem. Phys. Lett*., 2008, **461**, 238.

33 S. Shen, X. Wang, T. Chen, Z. Feng and C. Li, J. *Phys. Chem. C,* 2014, **118**, 12661.

Table 1 Properties of the TiO_2 photocatalysts studied

	Supplier	d (nm)	R/A
P25	Evonik Degussa	21	0.2
ST01	Ishihara Sangyo	7	0
ST21	Ishihara Sangyo	20	0
ST41	Ishihara Sangyo	200	0
F1	Showa Titanium	90	0.22
F2	Showa Titanium	60	0.26
F4A	Showa Titanium	30	<0.05
F6A	Showa Titanium	15	<0.05

Table 2 Values of $[I_{ex}]_{peak}$ and $[\Phi_{CG}\mu]_{max}$ for the TiO_2 photocatalysts studied

	d (nm)	$[I_{ex}]_{peak}$ (mJ s^{-2})	$[\Phi_{CG}\mu]_{max}$ (cm^2 V^{-1} s^{-1})
P25	21	0.01	0.015
ST01	7	0.2	0.002
ST21	20	0.003	0.007
ST41	200	~0.0001	0.05
F1	90	~0.0005	0.03
F2	60	0.001	0.015
F4A	30	0.007	0.008
F6A	15	0.05	0.003

Figures

Fig. 1 Schematic view of the sample cavity.

Fig. 2 $\Phi_{CG}\mu$ as a function of I_{ex} for the standard sample (ST) and a powder sample of P25 under the same experimental conditions.

Fig. 3 Decay profiles of the TRMC signal of P25 (I_{ex} = 1.3 mJ cm^{-2}) and ST01 (I_{ex} = 1.5 mJ cm^{-2}) before and after thermal treatment at 300 °C for 1 h.

Fig. 4 Decay profiles of $-(\Delta P/P)$ for the TiO$_2$ samples listed in Table 1 (I_{ex} = 2 mJ cm^{-2}).

Fig. 5 TRMC signals of G1 (Showa Titanium, d = 250 nm) and ST41 (Ishihara Sangyo, d = 200 nm).

Fig. 6 $\Phi_{CG}\mu$ as a function of I_{ex}.

Fig. 7 $[I_{ex}]_{peak}$ as a function of the particle diameter d.

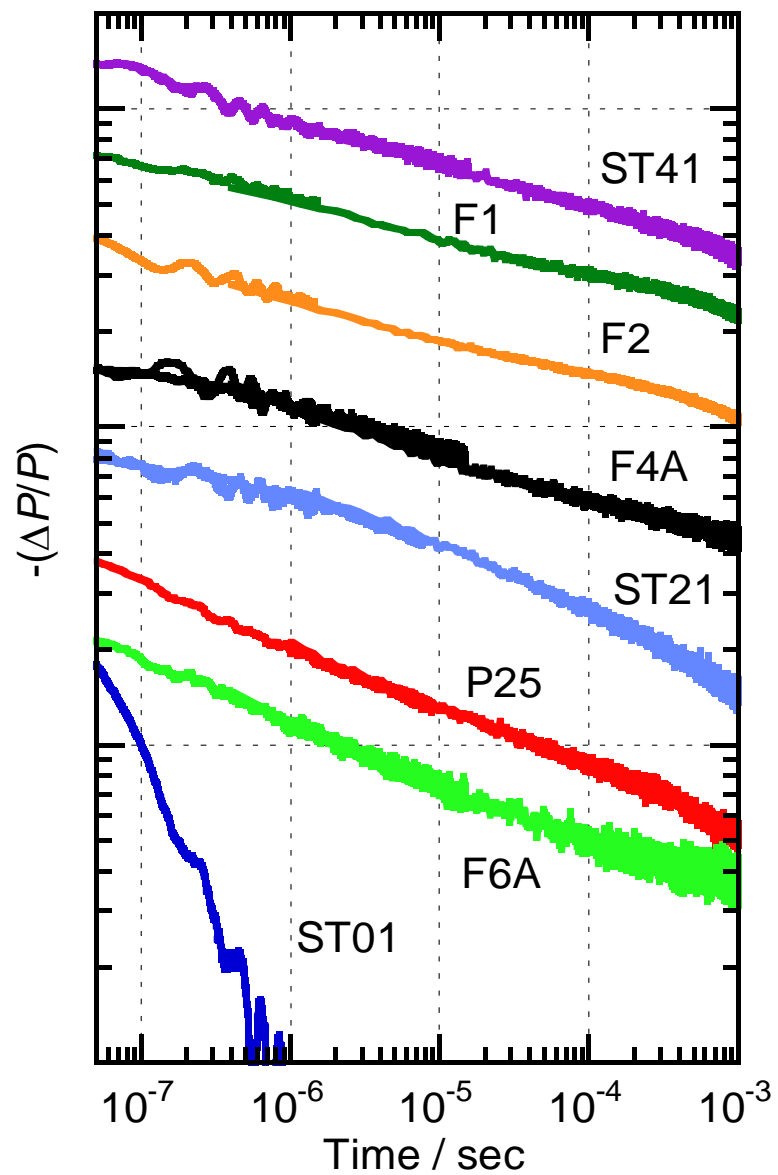Fig. 8 $[\Phi_{CG}\mu]_{max}$ as a function of the particle diameter d.
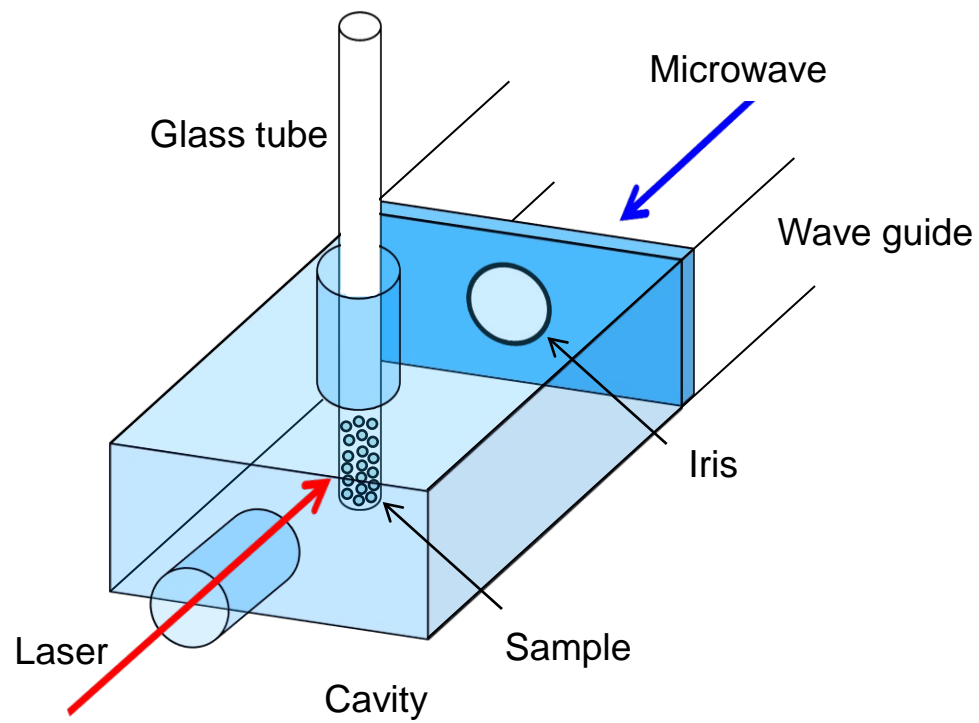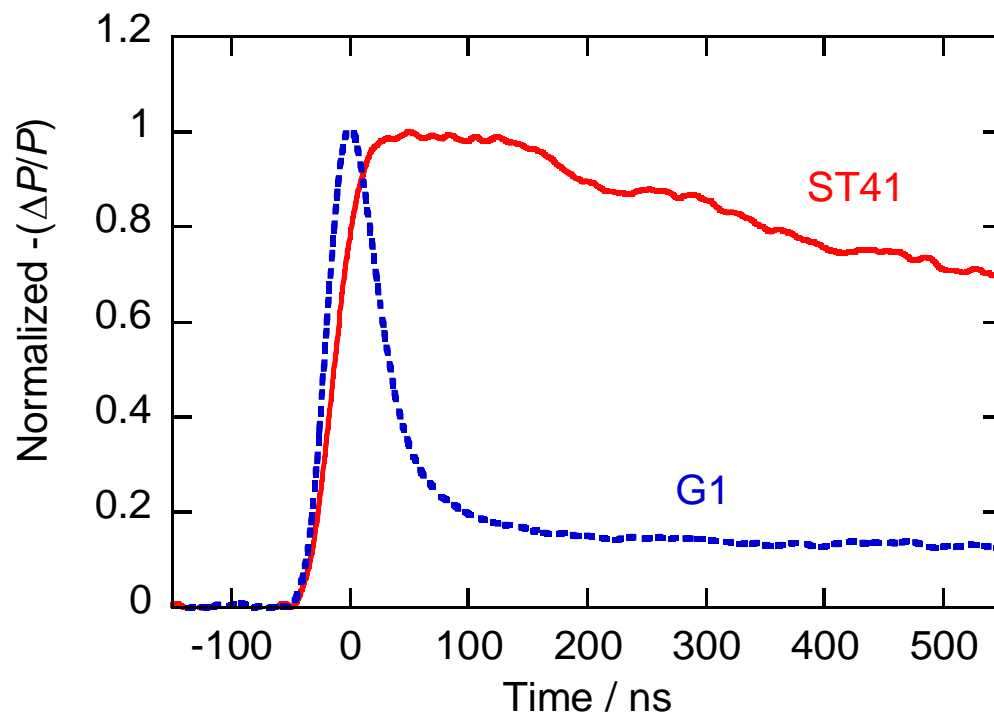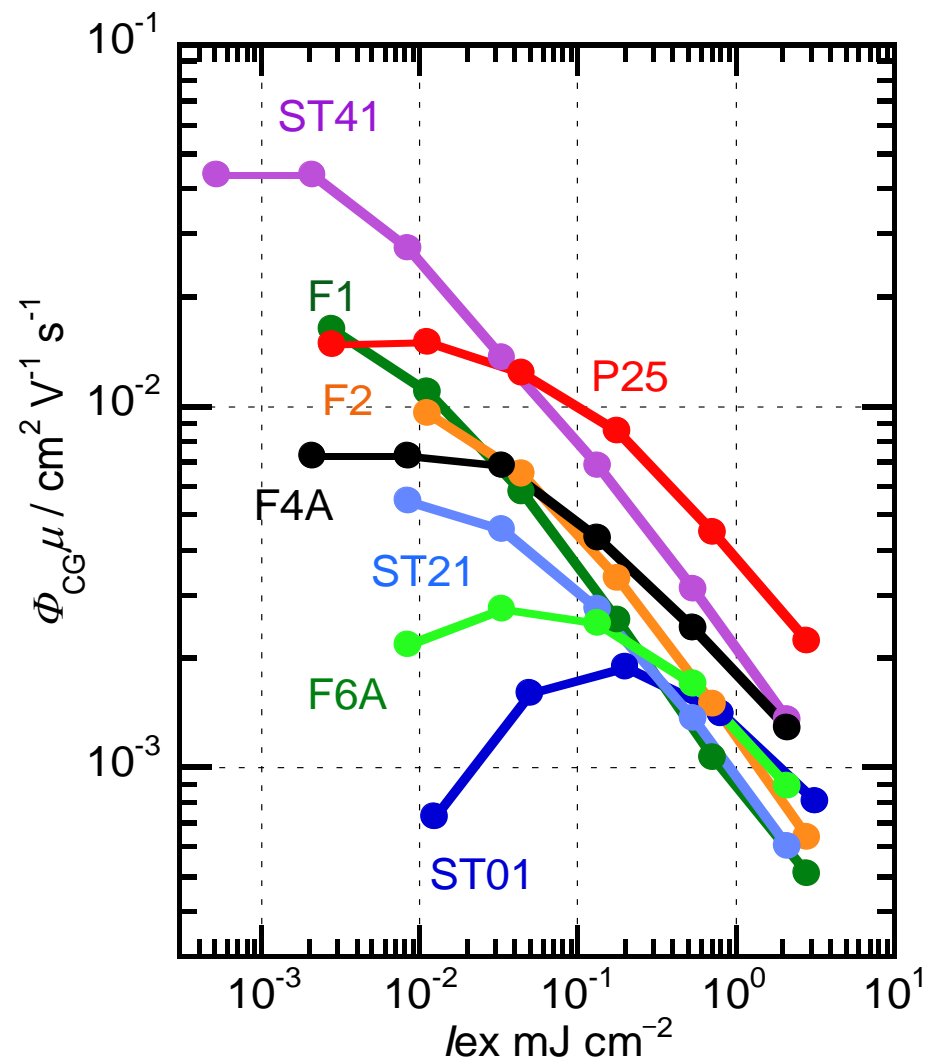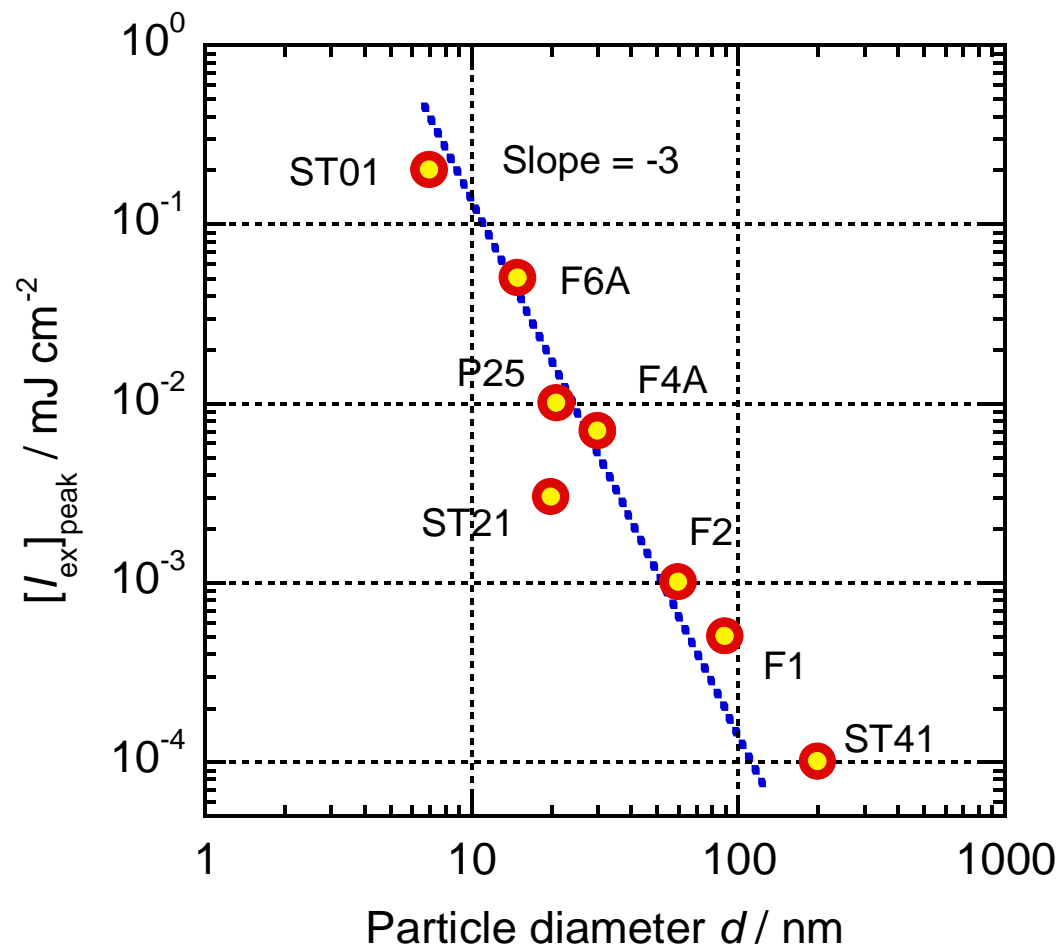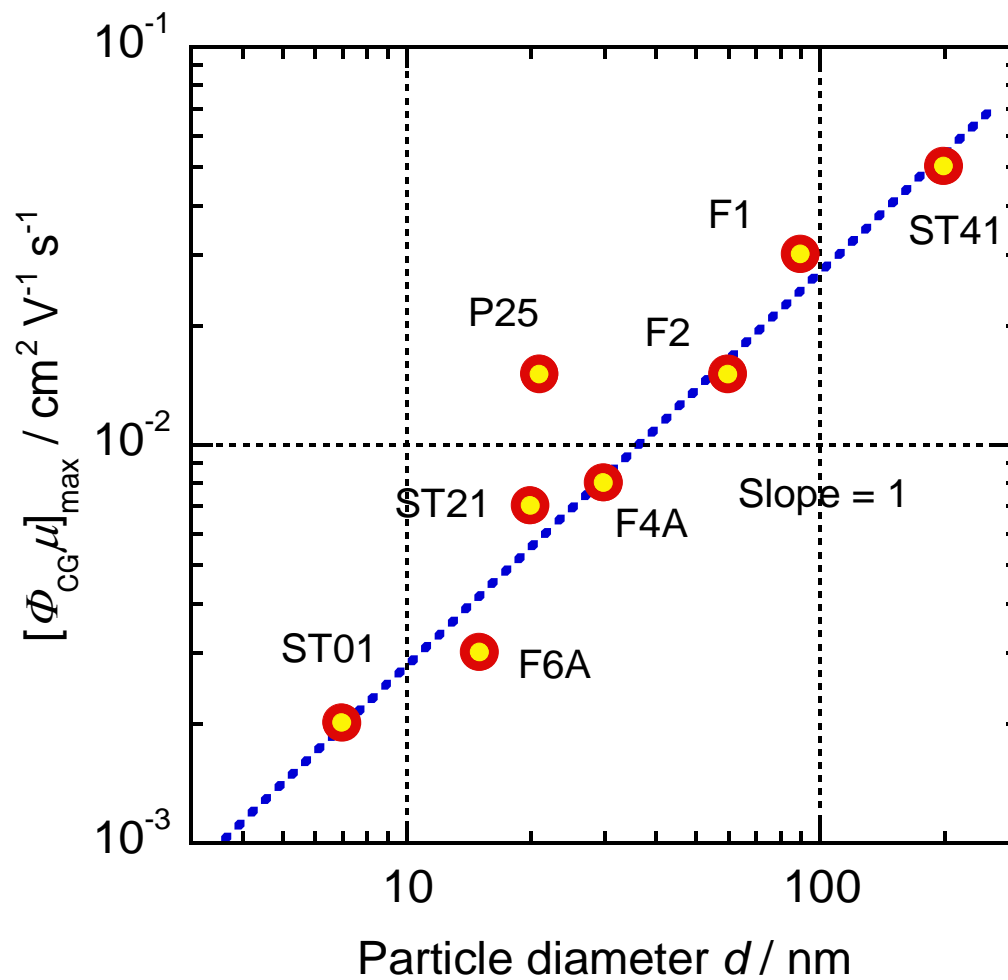
Fig. 1
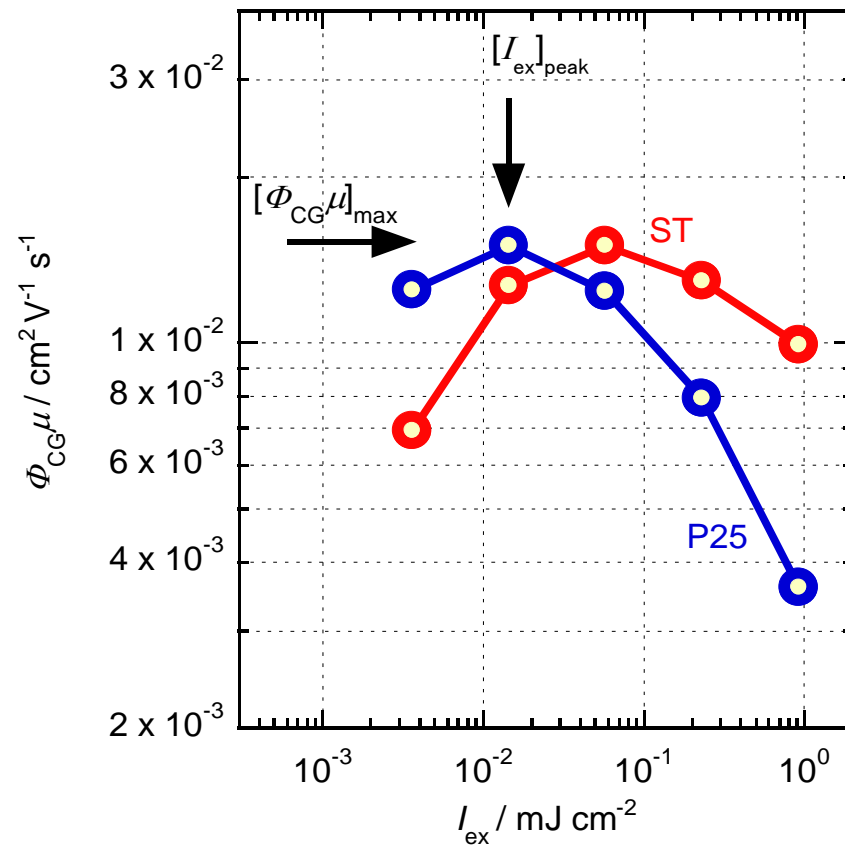
Fig. 2
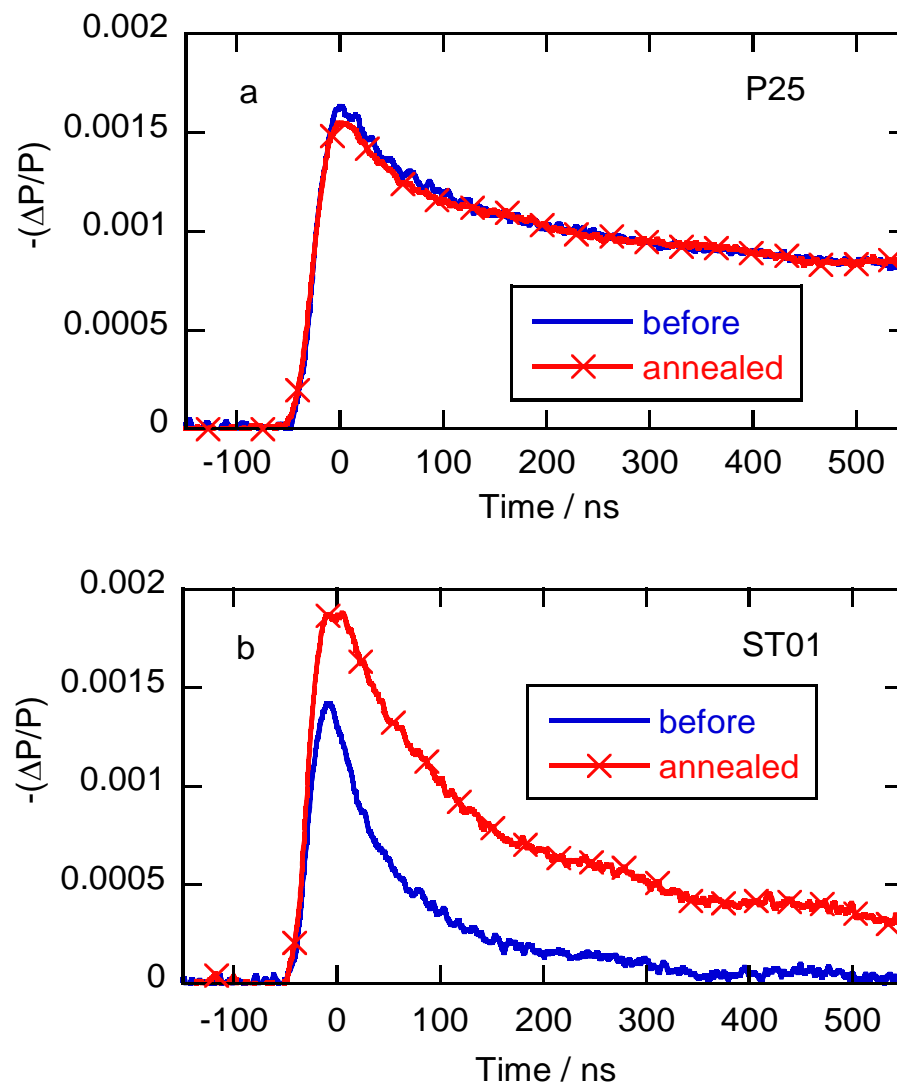
Fig. 3

Fig. 4

Fig. 5

Fig. 6

Fig. 7

Fig. 8

Graphical abstract